Curvature-surface analysis applied to a commercial and an academic injection system

Longxiang Huang, Diego Ferrando, Chetankumar S Vegad, F.X. Demoulin, Benjamin Duret, Julien Reveillon

Curvature-surface analysis applied to a commercial and an academic injection system

Longxiang Huang*[1], Diego Ferrando[1], Chetankumar S. Vegad[1], François-Xavier Demoulin[1], Benjamin Duret[1], Julien Reveillon[1]
[1]UMR 6614 - CORIA, University of Rouen Normandie, Saint-Étienne-du-Rouvray, France
*Corresponding author: huangl@coria.fr

Abstract
The primary break-up of an injection system results in the formation of non-spherical droplets and liquid ligaments. Depending on the Weber number, a secondary break-up may occur, resulting in the formation of smaller, spherical droplets. The droplet size distribution (DSD) is measured after the completion of the secondary break-up to obtain a high sphericity validation rate.
Numerical simulation of both break-ups using an Interface Capturing Method (ICM) is challenging due to the computational demands. The scale of the smallest droplets is typically 2 to 3 orders of magnitude smaller than the numerical domain, requiring a large number of computational elements. However, the ligaments and droplets formed during the primary break-up process contain valuable information about the final spray size distribution. Research by Palanti [1] proposed an analysis based on the curvature and surface area of the early atomization process to calculate the final DSD. This analysis was further extended by Ferrando [2] adding the capability to calculate the velocity of the droplets.
The curvature-surface analysis has been applied to a commercial simplex swirl atomizer [3] using Large-Eddy Simulation (LES) where the DSD was well captured in comparison with experiments [4]. However, the numerical simulation overestimated the joint velocity distribution of the droplets. This particular injector has a complex geometry and several physical processes are involved. The model and discretization schemes chosen play a role in solving the flow, therefore, the overestimation of the droplet velocity may be due to the flow downstream, and not the curvature analysis itself. To further study this analysis, this work uses a simpler academic case with a simpler geometry. A Direct Numerical Simulation is performed using the ARCHER code, in order to avoid using any turbulence model that may affect the final results. Unlike previous works which used the interFoam solver (volume of fluid-based solver), this study uses a more precise ICM called the level-set method. The curvature-surface analysis method is applied to evaluate its effectiveness.

Keywords
Curvature, Spray, Primary break-up, Simplex-swirl-atomizer, Drop-Size-Distribution

Introduction

In traditional practice, the measurement of spray characteristics, such as droplet diameter or droplet velocity, is performed at a considerable distance from the nozzle orifice to ensure the completion of the break-up process and the formation of fully spherical liquid structures. Experimental methodologies, such as phase Doppler anemometry (PDA), exhibit an enhanced validation ratio as they are implemented further away from the nozzle orifice [5]. Similar limitations are encountered in computational fluid dynamics (CFD) simulations when counting the number of droplets or converting them from an Eulerian formalism to a Lagrangian formalism [6, 7]. In such cases, droplets are required to possess a spherical morphology, which requires enlarging the numerical domain, and thus, increasing the simulation costs.
In recent years, a novel technique for investigating the near flow field to the nozzle has been proposed by [1] through a multiphase simulation using a Volume of Fluid (VOF) approach. The principal objective of this study was to scrutinize the curvature of liquid structures created near the nozzle to estimate the diameter distribution of the droplets. The investigation was carried out in an academic airblast atomizer and validated by comparing it with experimental results [8]. Subsequently, some studies have adopted this new approach to obtain spray characterization. For instance, [2] retrieved the velocity of the droplets, together with the Droplet Size Distribution (DSD), in another airblast atomizer.
The latest advancements in this field are concentrated on adapting the analysis to the experimental domain [5]. A significant disparity between simulations and experiments arises due to the fact that, in the former, the three-dimensional flow field is well-known in space and time. However, as stated in subsequent sections of this article, the data obtained from experiments only provides two-dimensional projections of liquid structures. Consequently, the analysis must be adapted to operate with 2D data rather than 3D data.
The objective of this study is to explain the mechanism of the curvature-surface analysis, its utilization in Computational Fluid Dynamics (CFD) and experiments, and to conduct a review of the validations that have been performed on a specific injector.

Curvature-surface analysis

As proposed by Palanti [1], it is plausible to derive the Droplet Size Distribution (DSD) of a spray that has completed the first break-up stage by calculating the curvature at the surface interface between gas and liquid. The distribution of curvatures at the surfaces of liquid structures, weighted by the amount of surface interface, is then used to compute the drop size distribution [9].

Initially, studies were carried out employing a Volume of Fluid-based solver (`interFoam` [10]). Consequently, the methodology was developed within the VOF framework. However, to enable the application of this analysis beyond this specific framework, several parameters needed to be defined.

The Phase Indicator (PI) quantifies the amount of liquid present in a discretized space. It is analogous to the Liquid Volume Fraction (LVF) or α in VOF solvers. Thus, within the VOF framework, it directly corresponds to the LVF. However, in a 2D projection (Projected Phase Indicator or PPI), it represents the ratio of liquid to gas within a discretized area. Other variables can be obtained from this parameter.

For the sake of simplicity, PI will be called α in equations from now on.

The curvature κ is defined as the inverse of the droplet diameter, $\kappa = 4/D$. In this study, the curvature is determined as the divergence of the normal vector to the surface interface, which is given by the following equation:

$$\kappa = \nabla \cdot \left(\frac{\nabla \alpha}{|\nabla \alpha|} \right) \tag{1}$$

However, there exist alternative definitions of curvature that can be employed using a framework different from PI. These alternative definitions must be explored and studied further.

The amount of surface interface between gas and liquid can be obtained as:

$$\Sigma = |\nabla \alpha| \tag{2}$$

In 3D, it corresponds to the ratio of the amount of surface to the control volume. In 2D, it represents the ratio of the amount of perimeter of the droplet to the control surface.

Equivalent Sauter Mean Diameter

To investigate the evolution of the break-up process, an equivalent length to the Sauter Mean Diameter (SMD or D_{32}) is defined as l_{32}. l_{32} is equivalent to the SMD when applied to a cloud of spherical droplets and provides an estimation when applied to a cloud of non-spherical liquid structures. l_{32} is defined as follows:

$$l_{32} = 6\frac{V_l}{A_l} = 6\frac{\int_T \iint_S (\alpha \boldsymbol{u} \cdot \boldsymbol{n} ds) dt}{\int_T \iint_S (\Sigma \boldsymbol{u} \cdot \boldsymbol{n} ds) dt} \tag{3}$$

l_{32} is the ratio of the liquid volume flux to the surface interface flux, both integrated in time and space in a given plane. The factor of 6 establishes the equivalence between the classic definition D_{32} [11] and this particular and more general definition.

$$D_{32} = \frac{\sum_i N_i D_i^3}{\sum_i N_i D_i^2} \tag{4}$$

When the analysis is applied to a 2D projected field, D_{32} cannot be estimated. Therefore, the characteristic diameter l_{21} is estimated using the same approach. The formula for l_{21} is as follows:

$$l_{21} = 4\frac{A_l}{P_l} = 4\frac{\int_T \iint_S (\alpha \boldsymbol{u} \cdot \boldsymbol{n} ds) dt}{\int_T \iint_S (\Sigma \boldsymbol{u} \cdot \boldsymbol{n} ds) dt} \tag{5}$$

In this case, the factor that makes both equations equivalent is 4.

It has been validated that l_{32} is a good estimation of the final l_{32} obtained from experiments [1, 2, 3] when the primary break-up is completed.

Surface Curvature Distribution (SCD)

The derivation of the drop size distribution (DSD) requires the initial recovery of the curvature distribution, which is subsequently weighted by the surface interface. As the approach proposed by [9], the DSD can be converted into the SCD. In this analysis the opposite conversion is made: from the curvature distribution weighted by the surface interface, the DSD is obtained.

It is worth noting that the methodology used to recover the curvature and surface interface density data may differ between studies. For numerical simulations, measurements have been taken by evaluating κ and Σ in each numerical cell within a predetermined box (as in the case of Palanti [1]), or in the face cells of a designated plane (as in the case of Ferrando[3]), which were later integrated over time. On the other hand, in experiments, due to the 2D projection of the data and the uncorrelated nature, on time, of snapshots, the methodology employed involved in measuring the data is like the one used in the first case, a predefined box.

Drop Size Distribution (DSD)

To recover DSD from SCD, certain assumptions and estimations are necessary. This analysis assumes that the surface interface recovered corresponds to a spherical droplet, and its diameter is a function of the curvature. Consequently, the number of droplets can be calculated as a function of diameter using the following equation:

$$D(\kappa) = 4/\kappa \tag{6}$$

The diameter of the spherical droplet is directly proportional to the inverse of the curvature. Specifically, the diameter can be calculated as four times the inverse of the curvature.

$$n(\kappa) = \frac{S_T(\kappa)}{\pi D(\kappa)} \tag{7}$$

being $S_T(k)$ the total surface recovered for a particular value of κ.
The number of droplets can be determined by dividing the total surface interface, as a function of curvature, by the surface area of a spherical droplet with a diameter of $D(k)$.

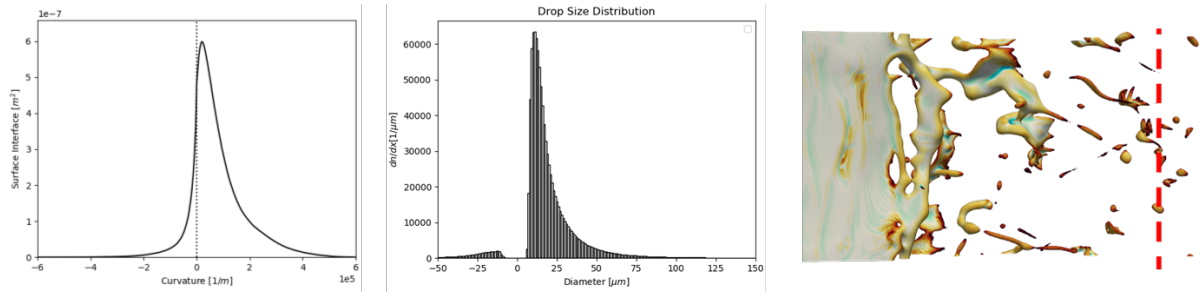

Figure 1. Left to right: Surface Curvature Distribution, Drop Size Distribution, Iso-Contour ($\alpha = 0.5$) with the curvature κ coloured on it. Raw results after applying the analysis.

This assumption of spherical droplets corresponding to the surface interface in near-field regions is only an approximation. Figure 1 shows the SCD, DSD, and an iso-contour of α in 3D coloured by the curvature (blue $\kappa < 0$, red $\kappa > 0$ and white $\kappa = 0$). There is some surface interface corresponding to negative curvatures, which corresponds to bubbles or concave liquid structures, rather than spherical droplets. Therefore, the initial correction to this procedure is to eliminate the surface interface of negative curvatures and thus, the "droplets" with negative diameters.

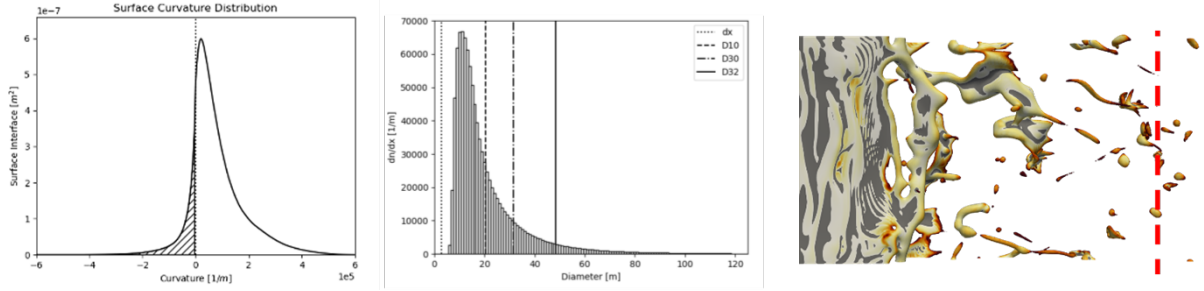

Figure 2. Left to right: Surface Curvature Distribution, Drop Size Distribution, Iso-Contour ($\alpha = 0.5$) with the curvature κ coloured on it. Results after removing negative curvature values.

Figure 2 shows the SCD, DSD, and the iso-contour of Figure 1 with the initial correction already applied. In this instance, the iso-contour is coloured grey in the regions where the surface corresponds to negative curvatures. The measurement plane is represented by the red line, nearly all surfaces are recovered and not removed. However, as evident from the DSD, there exist a small number of excessively large droplets corresponding to near-zero curvatures. These droplets are unphysical since they correspond to almost flat elements that are not close to spherical droplets. To resolve this issue, the D_{32} calculated with l_{32} is imposed in the DSD since it is a reliable value, as previously demonstrated. As a result, the largest droplets are removed from the distribution until the D_{32} calculated using Equation 4 in the DSD and the l_{32} calculated with Equation 3 are identical.
Figure 3 shows the final outcome of the approximations. The corrections made have been verified against experimental results and empirical equation [1, 2, 3].
To apply it in 2D projected cases some adaptations are done:

1. The diameter is 2 times the inverse of the curvature: $D(\kappa) = 2/\kappa$

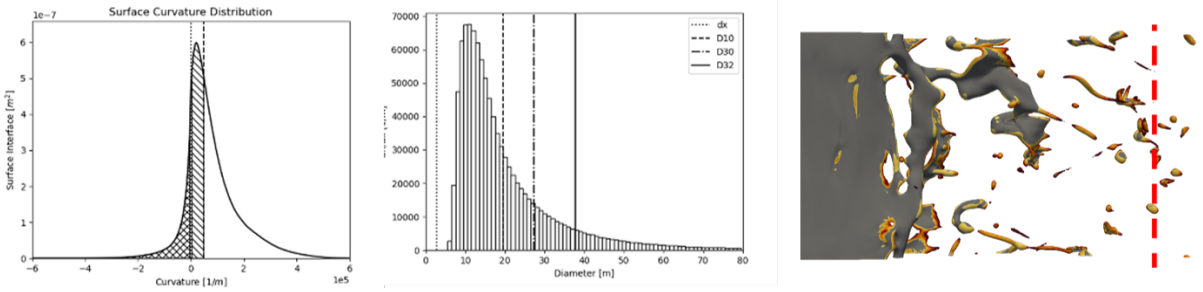

Figure 3. Left to right: Surface Curvature Distribution, Drop Size Distribution, Iso-Contour ($\alpha = 0.5$) with the curvature κ coloured on it. Results after removing large droplets.

2. The number of droplets is calculated with the perimeter of one droplet: $n(\kappa) = \dfrac{P_T(\kappa)}{\pi D(\kappa)}$

3. The corrections on the DSD are done using the l_{21} instead of l_{32}.

Simplex Swirl Atomizer Configuration

The present study focuses on investigating the spray formed by the *Coria Rouen Spray Burner (CRSB)* injector, which is a simplex swirl atomizer. This injector has been the subject of several previous works[12, 13, 5], where PDA measurements were conducted to characterize its behaviour.
To obtain the necessary data for the curvature-surface analysis, both the experimental and numerical setups are described in this section.

Experimental set-up

The CORIA Rouen spray burner (CRSB) was adopted to atomize n-heptane fuel. The burner comprises the fuel injection system and plenum. The fuel injector is located at the top of the injection system and surrounded by a co-flow air stream guided through a convergent annular passage. The downstream end of the annular passage is 20 mm outer diameter and 10 mm inner diameter. While its upstream end is connected to the plenum housing 18 radial vanes of zero-degree angle. The purpose of providing radial vanes is to break large flow structures. Further details on burner geometry are available in [12].

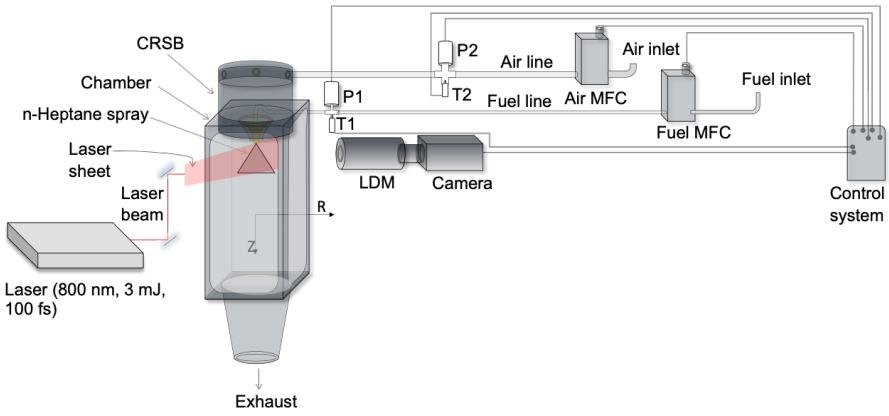

Figure 4. The schematic of the experimental setup demonstrating the instruments and optics arrangement for 2p-LIF technique. The numbers 1 and 2 correspond to n-heptane and air, MFC-mass flow controller, LDM-long distance microscope, T-thermocouple, P-pressure transducer, Z-axial direction, and R-radial direction.

In Fig. 4, Z and R represent the axial and radial directions, respectively. The spray formation is in the downward (positive Z) direction. An industrial pressurized swirl injector (Danfoss make) of 80° hollow cone, 1.35 kg h^{-1} flow rate and 200 μm orifice diameter was used for n-heptane atomization. An internal geometry of the injector is such that an extent of fuel pressure is utilized to form a rotating liquid film leading towards the orifice, while the remaining fuel pressure is applied to force the liquid through an orifice as a conical sheet into the air. N-heptane mass flow rate was 0.28 g s^{-1} and regulated using Coriolis mass flow controller (Bronkhorst, CORI-FLOW, 0-2 g s^{-1}). The air mass flow rate was set to 6 g s^{-1} and controlled by a thermal mass flow controller (Bronkhorst, EL-FLOW, 0-15 g s^{-1}). The temperature of n-heptane and air were measured using K-type thermocouples (T1 and T2), and their pressures were measured using pressure transducers (P1 and P2).
To perform 2p-LIF experiments, a regenerative amplified Ti:Sapphire (Coherent Inc.) laser system of 800 nm wavelength, 3.5 mJ pulse^{-1} energy, 1 kHz repetition rate, and 100 fs pulse duration was used. The laser beam exhibits a 5 mm full width at half maximum (FWHM) Gaussian profile. A cylindrical lens was employed to form a $\sim$50 μm

thin laser sheet illuminating fuel-tracer solution spray. After absorption, the excited tracer molecules jump to higher energy states and decay to lower states by emitting fluorescent photons. An ICCD camera (PiMAX 4, 1024 $\times$ 1024 pixels^2) was orthogonally positioned to collect fluoresced light (emission) from the spray. Microscopic imaging was preferred in the present study [14] as the primary breakup of the n-heptane conical sheet is at about 1 mm axial distance from the nozzle exit. Thus, a long-distance microscope (LDM, QM-100, Questar) was equipped with a camera to capture a 2.5 $\times$ 2.5 mm^2 field of view at the nozzle exit.
A direct measurement of drop size was carried out using a phase Doppler anemometry (PDA) system (Dantec make). The purpose of PDA measurement is to compare drop size distribution (DSD) predicted from the curvature analysis of numerical and experimental data. In PDA arrangement, green (514.5 nm) and blue (488 nm) argon laser beams (2.2 mm diameter and 38 mm spacing) were utilized for measurements. The focal lengths of the transmission and receiver lenses were 350 mm and 310 mm, respectively. Beam crossing resulted in a probe volume of 0.148 $\times$ 0.148 $\times$ 3.10 mm^3. The receiver probe was set at θ = 70° off-axis angle in front scattering mode. It is close to Brewster's angle for n-heptane (refractive index, n = 1.392). It helps to reduce the effect of trajectory ambiguity while collecting reflected and refracted light by the receiver probe. The acquisition was started from Z = 1 mm downstream of the injector orifice and limited by 30 seconds or 1,20,000 droplets to achieve convergent statistics.

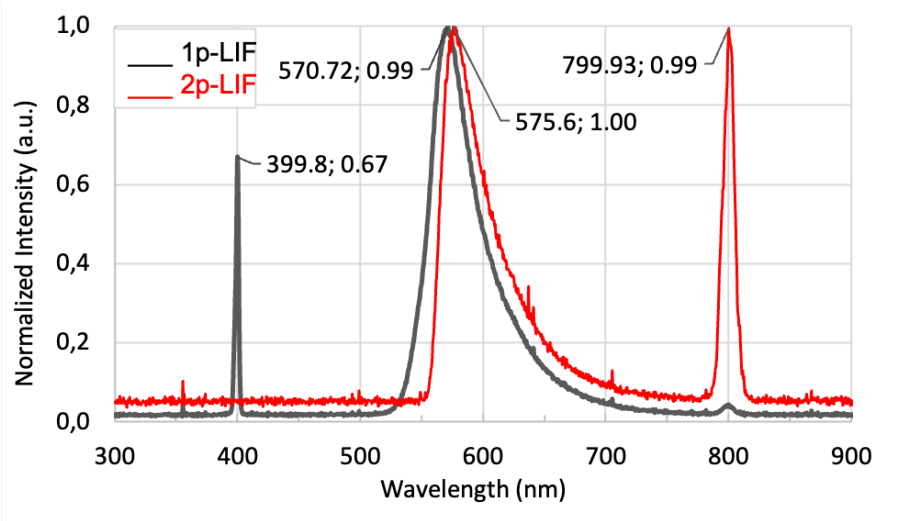

Figure 5. 1p-LIF and 2p-LIF emission spectrum of n-heptane fuel and PM-567 tracer dye solution. The gray and black lines correspond to 1p-LIF and 2p-LIF techniques, respectively. The peak emissions of 1p- and 2p-LIF when excited with 400 nm and 800 nm laser lights are ∼570 nm (gray line) and ∼576 nm (black line).

It was challenging to find a tracer dye for n-heptane fuel in terms of 2p-LIF technique. Common tracers for water or amines are fluorescein, eosin, Rhodamine 6G, and many [15, 16]. None of these dyes are soluble in non-polar alkanes, i.e., n-heptane. Further, very few tracer dyes for n-heptane fuel are noted in the existing literature. Adding a small amount of organic compound such as alcohol may help to dissolve polar (i.e., eosin) or slightly polar (i.e., Nile red) tracer into non-polar fuel (i.e., n-heptane). Durst et al. [14] added 20% propanol to dissolve eosin Y salt (60 mg l^{-1}) in n-heptane. Adding a small percentage of ethanol into n-heptane and Nile red solution results in a maxima shift in the emission spectrum [14, 17]. Thus, adding organic compounds can increase the tracer solubility or emission, but it may also change fuel properties. However, this is not the case here. No organic compound was added during the solubility test of various dyes in n-heptane.
The solubility test for solvent n-heptane was performed for the fluorescein-548 (F-548), pyrromethene-597 (PM-597), pyrromethene-567 (PM-567), and coumarin-504T (C-504T). All the dyes tested here are in the solid phase and nontoxic. In comparison, coumarin-504T did not dissolve entirely as some solid particles were observed at the bottom of the solution. However, the other two dyes pyrromethene-567 and pyrromethene-597 were seen to be completely soluble in n-heptane.
For each tracer dye, a fuel-tracer solution was prepared with 0.5 % by weight dye concentration in the n-heptane. The solution was kept in a quartz cuvette and excited with 400 nm and 800 nm laser lights to measure fluoresce characteristics of 1p-LIF and 2p-LIF respectively. The 400 nm laser light was produced by placing a frequency-doubling crystal in an 800 nm laser light path. PM-567 is used as a tracer dye for n-heptane fuel in the present study. The 1p-LIF and 2p-LIF emission spectrum for PM-567 and n-heptane solution is shown in Fig. 5. The measured peak emission ($\lambda_{max,fl}$) for 2p-LIF is ∼576 nm at peak absorption ($\lambda_{max,abs}$) of 800 nm. Similarly, in the case of 1p-LIF, the peak emission ∼571 nm is noted for 400 nm excitation. Both the peaks are marked in Fig. 5. It is to be noted that a part of the excitation wavelengths was directed toward the probe to show the absorption wavelengths in Fig. 5. The theory of two-photon absorption is available in [18, 19].

Simulation set-up

Previous works on the Coria Rouen Spray Burner (CRSB) injector have included numerical modelling, with studies conducted by [2, 4, 3] presenting detailed analyses of the injector's multiphase modelling. Interested readers are

directed to consult these references for further information.
In this article, a brief summary of the numerical simulation performed is provided. Experimental measurement techniques were employed to measure the internal 3D geometry of the injector's metallic pieces. Then, a hybrid tetrahedral-hexahedral mesh is generated. This mesh allows for high-resolution modelling in the zone of interest while using a tetrahedral approach in areas where mesh parameters are insufficient, thereby minimizing numerical instabilities.
The internal multiphase flow of the injector is solved using a Volume of Fluid (VOF) based method within the `OpenFOAM` toolbox, specifically the `interFoam` solver. The solved equations are:

$$\frac{\partial \bar{u}_j}{\partial x_j} = 0 \tag{8}$$

$$\frac{\partial \bar{\rho}\bar{u}_i}{\partial t} + \frac{\partial}{\partial x_i}(\bar{\rho}\bar{u}_j\bar{u}_i) = -\frac{\partial \bar{P}}{\partial x_i} + \frac{\partial}{\partial x_j}\left(\tau_{ij} + \tau_{tij}\right) + \bar{\rho}g_i + f_{\sigma i} \tag{9}$$

where $\bar{u}$ represents the velocity vector, $\bar{P}$ the pressure, $\bar{\rho}$ the density of the cell mixture (defined as $\bar{\rho} = \bar{\alpha}\rho_l + (1 - \bar{\alpha})\rho_g$, τ_{ij} and τ_{tij} the viscous and turbulent stresses including all sub-grid scale effects.
Additionally, g_i the gravitational acceleration, whereas f_σ represents the surface tension forces, calculated as:

$$f_\sigma = \sigma\kappa\frac{\partial \bar{\alpha}}{\partial x_j} \tag{10}$$

where σ is the surface tension between the liquid and the gas, α is the liquid volume fraction and κ is the curvature of the surface interface.
In order to determine the interface position, an equation for the liquid volume fraction α advection is solved:

$$\frac{\partial \bar{\alpha}}{\partial t} + \frac{\partial(\bar{\alpha}\bar{u}_j)}{\partial x_j} + \frac{\partial(U_j^r\bar{\alpha}(1-\bar{\alpha}))}{\partial x_j} = 0 \tag{11}$$

In addition, a Large Eddy Simulation (LES) framework was adopted, with the WALE sub-grid scale model retained from the internal simulation.
However, the atomization process was not adequately captured due to the low mesh resolution above the nozzle. To address this, a second simulation was conducted on a smaller but more refined numerical domain beginning at the nozzle orifice. In this simulation, the velocity vector $\mathbf{u}$ and the liquid volume fraction α were recovered from the first simulation and mapped onto the refined domain to achieve better qualitative agreement with experimental results.
In the second configuration, which involves external flow simulation, the curvature κ, surface interface density Σ, and liquid volume fraction α are obtained to apply the curvature-surface analysis.
Figure 6 shows a central slice of the external flow simulation domain. On it, the black dashed lines represent the planes where the flux of α and Σ are stored to later calculate l_{32} with Equation 3. The red line represents the plane where κ and σ are stored to calculate first, the SCD and derive from it the DSD.

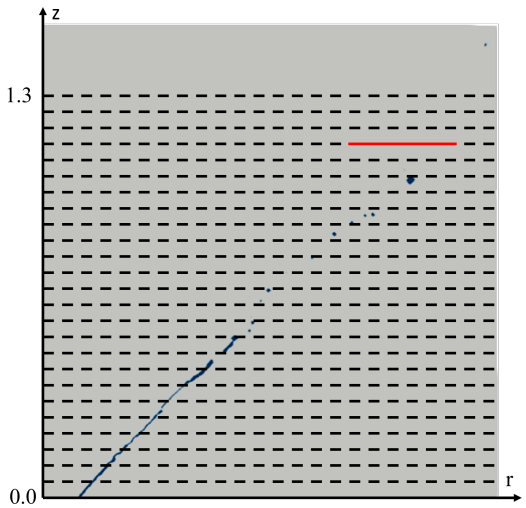

Figure 6. The liquid volume fraction contour is presented with dashed black lines indicating the planes where the surface interface and liquid volume fraction data are stored for computing the equivalent Sauter Mean Diameter (SMD). The red line denotes the region where the probes are setup to obtain measurements of the Droplet Size Distribution (DSD)

Results

In Figure 7, l_{21} (Equation 5) is computed along the axial distance to the injector using 2p-lif images. Each l_{21} value is computed on one window of the image for a size of $128x1024$ pixels, counting a total number of 15 windows with a step size of 64 pixels for each time we step towards the bottom of the image. In Figure 7 b, the drop size distribution is computed on the last window of 2p-lif images with the same parameters used in while calculating l_{21}. Both, the drop size distribution and l_{21} computed on the last window match the PDA measurement results. However, this correspondence depends on the treatment of the raw images before applaying the curvature-surface analysis.

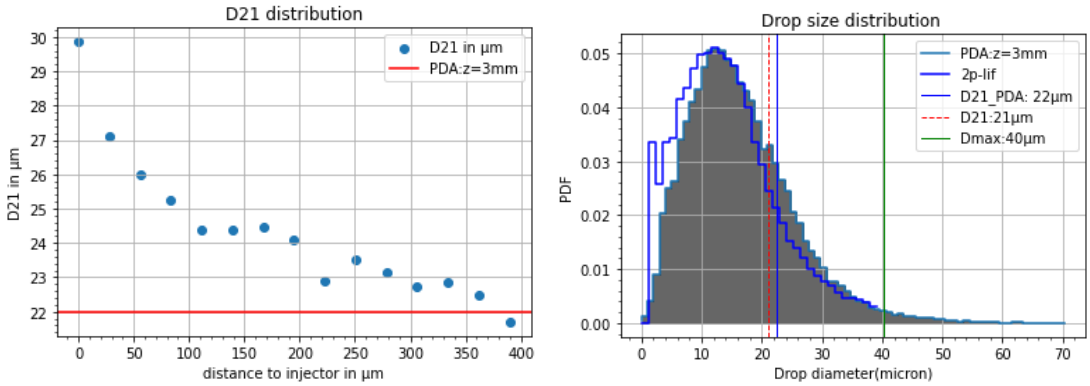

Figure 7. On the left: l_{21} in function of the axial coordinate calculated using 2p-lif images. On the right: drop size distribution of the 2p-lif images

Figure 8 shows Equation 3 applied to the numerical computation in the planes reported in Figure 6. At $z = 0mm$, l_{32} gives a high value not corresponding to a physical D_{32}. This value is obtained at the nozzle where the break-up process has not begun yet and, hence, the calculated value corresponds to a corona-like surface. When the liquid sheet begins breaking-up, more ligaments and smaller liquid structures appear generating more surface interface. l_{32} is then going down up to a point where it reaches an almost constant value ($z \approx 0.2mm$). At this point, most of the break-up process is completed, and the remaining process that is yet to finish will not generate a considerable amount of surface interface that will vary the l_{32} value. Therefore, from this point to the last measured plane ($z = 1.3mm$), the approximation to D_{32} is considerably accurate. The figure shows a small increase tendency of l_{32} from $z = 0.2mm$ to $z = 1.3mm$. This effect was noticed in experiments by [13]. The value at $z = 1.2mm$, where the DSD is calculated, is $l_{32} = 28\mu m$ which is reasonably similar to PDA measurements $D_{32} = 26\mu m$.

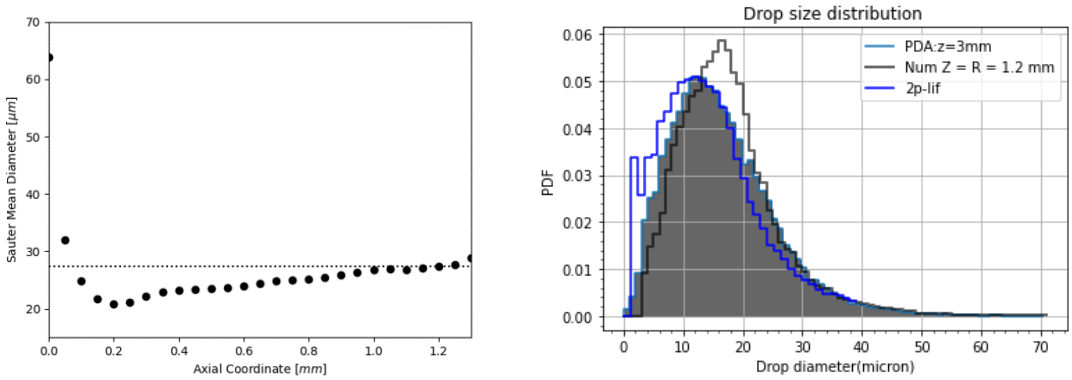

Figure 8. On the left: l_{32} evolution on axial coordinate obtained by numerical simulation. On the right: Drop size distribution comparison between PDA and curvature analysis applied on numerical simulation and 2p-lif images

In Figure 8 the drop size distribution obtained with three different methods is shown. The PDA measurements in grey are the reference value to validate the curvature-surface analysis applied to the studied of this work. The CFD results are in agreement with both, PDA measurements and DSD obtained through 2p-lif images.

Conlcusions

Curvature-surface analysis has been applied in several configurations and both, in experiments and numerical simulations, giving promising results. The analysis estimates accurately characteristics diameters such as D_{32} and D_{21} and it is capable of reconstructing a similar drop size distribution in the early stages of the atomization process. So far, the analysis has been applied over VOF simulations and 2pLIF pictures following a similar approach to VOF. The methodology could be adapted to other formalisms and high-accuracy numerical methods to enhance its capabilities.

Thus, more accurate interface capturing methods, such as Level-Set method (LS), may be used to calculate the curvature and surface interface density. Higher-order discretization schemes and Direct Numerical Simulations (DNS) should be tested in order to reduce any numerical errors to corroborate the great benefits of using this technique to calculate the DSD in a stage where the droplet cloud is not fully formed.
In experiments, the treatment of the raw 2p-lif images has demonstrated an influence on the final results. Guidelines to apply the correct filters and parameters should be proposed in the future to be consistent with the methodology.

Acknowledgements
Authors from Université de Rouen Normandie thankfully acknowledge the computer resources at IDRIS, TGCC and CINES under the allocation A0112B06153 and A0092B06153 made by GENCI (Grand Equipement National de Calcul Intensit) and also for the computing time at CRIANN (Centre Régional Informatique et d'Applications Numériques de Normandie) under the scientific project No. 2006011.

Nomenclature

α	Liquid Volume Fraction or PI [-]
κ	Curvature [m^-1]
Σ	Surface Interface Density [m^-1]
n	Number of droplets [-]
D_{32}	Sauter Mean Diamater [-]
l_{32}	Equivalent Sauter Mean Diamater [-]
$\mathbf{u}$	Velocity vector [m/s]
$\mathbf{n}$	Normal vector to the surface [-]

References

[1] Palanti, L., Puggelli, S., Langone, L., Andreini, A., Reveillon, J., Duret, D. and Demoulin, F.-X., 2022, *International Journal of Multiphase Flow*, 147.
[2] Ferrando, D., Palanti, L., Demoulin, F.-X., Duret, B. and Reveillon, J., 2021, 15th Triennial International Conference on Liquid Atomization and Spray Systems, Edinburgh, UK Edinburgh.
[3] Ferrando, D., Carreres, M., Belmar-Gil, M., Cercelló-Sanz, D., Duret, B., Reveillon, J., Salvador, F., Demoulin, F.-X., 2023, *Atomization and Sprays*.
[4] Ferrando, D., Vegad, C., Idlahcen, S., Vandel, A., Renou, B., Godard, G., Cabot, G., Blaisot, J., Duret, B., Reveillon. J., Demoulin, F.-X., 2022, 31th Conference on Liquid Atomization and Spray Systems, Virtual.
[5] Vegad, C., Ferrando, D., Idlahcen, S., Vandel, A., Renou, B., Godard, G., Cabot, G., Blaisot, J., Duret, B., Reveillon. J., Demoulin, F.-X., 2022, 31th Conference on Liquid Atomization and Spray Systems, Virtual.
[6] Warncke, K., Gepperth, S., B.Sauer, Sadiki, A., Janicka, J., Koch, R., Bauer, H.-J., 2017, *International Journal of Multiphase flow*, 91.
[7] Braun, S., Wieth, L., Holz, S., Dauch, T. F., Keller, M. C., Chaussonnet, G., Gepperth, S., Koch, R., and Bauer, H.-J., 2019, *International Journal of Multiphase flow*, 114.
[8] Gepperth, S., Guildenbecher, D., Koch, R., and Bauer, H.-J., 2010, In 23rd Annual Conference on Liquid Atomization and Spray Systems.
[9] Canu, R., Puggelli, S., Essadki, M., Duret, B., Menard, T., Massot, M., Reveillon, J., and Demoulin, F.-X., 2018.*International Journal of Multiphase Flow*, 107.
[10] Deshpande, S., Anumolu, L., and Trujillo, M, 2012. *Computational science and discovery*, 5(1).
[11] Lefebvre, A. H. and McDonell, V. G., 1988. Atomization and Sprays. *CRC Press Taylor and Francis Group*.
[12] Verdier, A., 2017. PhD thesis, Université de Rouen Normandie, France.
[13] Marrero, J., 2018. PhD thesis, Université de Rouen Normandie, France.
[14] Durst, M. Wensing, and E. Berrocal, 2018, *Applied Optics*, 57.
[15] E. Berrocal, E. Kristensson, and L. Zigan, 2018, *International Journal of Spray and Combustion Dynamics*, 10.
[16] M. Storch, Y. N. Mishra, M. Koegl, E. Kristensson, S. Will, L. Zigan, and E. Berrocal, 2016, *Optics Letters*, 41.
[17] P. Greenspan and S. D. Fowler, 1985 *Journal of Lipid Research*, 26.
[18] M. Pawlicki, H. A. Collins, R. G. Denning, and H. L. Anderson, 2009, *Angewandte Chemie-International Edition*, 48.
[19] P. T. C. So, C. Y. Dong, B. R. Masters, and K. M. Berland, 2000, *Annual Review of Biomedical Engineering*, 2.